MLLMs Need 3D-Aware Representation Supervision for Scene Understanding

Xiaohu Huang[1] **Jingjing Wu**[2] **Qunyi Xie**[2] **Kai Han**[1]*
[1] Visual AI Lab, The University of Hong Kong
[2] Department of Computer Vision Technology (VIS), Baidu Inc.
huangxiaohu@connect.hku.hk, jingjingwu_hit@outlook.com
xiequnyi@baidu.com, kaihanx@hku.hk

Abstract

Recent advances in scene understanding have leveraged multimodal large language models (MLLMs) for 3D reasoning by capitalizing on their strong 2D pretraining. However, the lack of explicit 3D data during MLLM pretraining limits 3D representation capability. In this paper, we investigate the 3D-awareness of MLLMs by evaluating multi-view correspondence and reveal a strong positive correlation between the quality of 3D-aware representation and downstream task performance. Motivated by this, we propose 3DRS, a framework that enhances MLLM 3D Representation learning by introducing Supervision from pretrained 3D foundation models. Our approach aligns MLLM visual features with rich 3D knowledge distilled from 3D models, effectively improving scene understanding. Extensive experiments across multiple benchmarks and MLLMs—including visual grounding, captioning, and question answering—demonstrate consistent performance gains. Project page: https://visual-ai.github.io/3drs

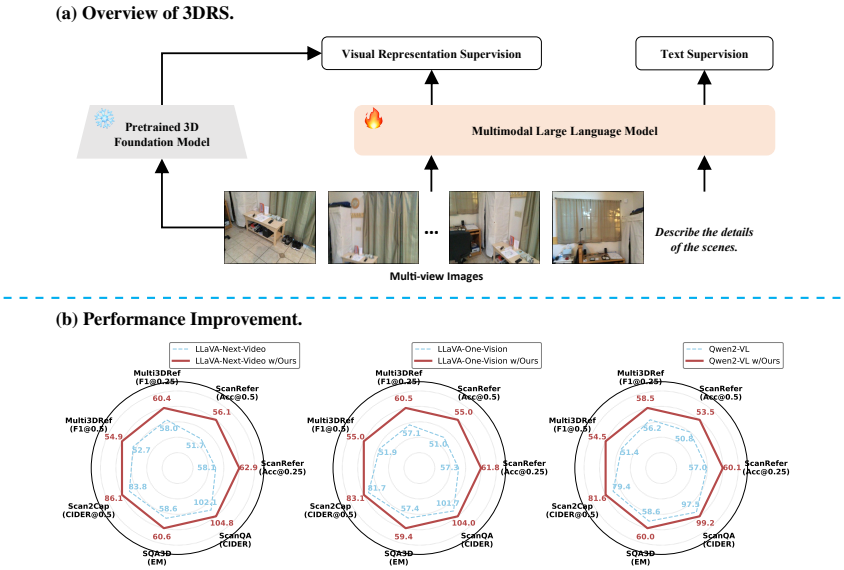

Figure 1: **Enhancing 3D awareness of MLLMs to improve downstream performance.** (a) Besides the common text supervision for MLLMs, 3DRS adopts 3D foundation models to supervise 3D-aware visual representation learning in MLLMs. (b) Combined with 3DRS, we achieve consistent performance improvement across multiple MLLMs and benchmarks.

*Corresponding author.

Preprint. Under review.

1 Introduction

Scene understanding serves as a cornerstone for interpreting 3D environments, enabling a wide range of critical applications ranging from robotic navigation to augmented reality. The recent emergence of large language models (LLMs) [41, 14, 15] has sparked innovative research aimed at endowing these models with scene comprehension capabilities. One major line of research [40, 20, 31, 16, 20, 34, 35, 8, 11, 7, 43] utilizes point cloud encoders—either independently or in combination with multi-view images—to extract 3D representations, which are subsequently projected into a language-aligned space for LLMs. However, these approaches are constrained by the scarcity of paired 3D-text datasets, which impedes effective cross-modal feature alignment.

In response to this challenge, recent state-of-the-art methods [50, 48, 13, 19, 32] have shifted towards leveraging multi-view images exclusively, drawing inspiration from the success of large-scale visual-language pretraining in multimodal LLMs (MLLMs) [25, 23, 46, 29, 38, 1]. These approaches aim to transfer 2D visual understanding to 3D scene comprehension by injecting 3D priors, such as 3D positional embeddings, into the models, thereby allowing MLLMs to capitalize on their extensive pretrained 2D knowledge for 3D interpretation.

Despite these advancements, genuine 3D scene understanding fundamentally requires models to capture intrinsic 3D attributes and spatial structures to comprehend scenes. The absence of explicit 3D data during MLLM pretraining reveals a significant gap, which motivates our core investigation centered around the following questions: (1) *How can we evaluate the ability of MLLMs to learn 3D-aware representations?* (2) *How does the quality of 3D feature learning influence downstream scene understanding performance?* (3) *What methods can enhance 3D-aware representation learning within MLLM frameworks?* While several prior works [42, 24, 12, 28] have attempted to probe the 3D awareness of 2D vision foundation models, systematic investigation into 3D-aware representation learning in MLLMs remains largely unexplored. This gap is particularly crucial given the growing adoption of MLLMs in multimodal 3D understanding tasks. Our study aims to address this overlooked area and provide new insights into 3D representation learning within the MLLM paradigm.

For the first question, we conduct comprehensive experiments to evaluate the 3D awareness on three representative MLLMs, including LLaVA-Next-Video [46], LLaVA-One-Vision [23], and Qwen2-VL [38], following the finetuing settings of Video-3D LLM [48]. Specifically, we assess 3D awareness via view equivariance, quantifying it by computing the feature similarity between corresponding pairs from the same 3D voxel across different views. This evaluation requires MLLMs to associate the same object across multiple views, thereby reflecting their capacity for 3D representation. Our analysis encompasses five datasets spanning tasks such as 3D grounding [4], captioning [9], and question answering [2].

To address the second question, we systematically analyze model performance across these datasets and observe that *samples with higher correspondence scores—i.e., those exhibiting stronger 3D awareness—consistently lead to improved performance.* This finding demonstrates a strong positive correlation between the quality of 3D-aware representations and downstream scene understanding performance, highlighting the necessity of enhancing 3D feature learning in MLLMs.

In response to the third question and building upon our earlier findings, we first introduce a view equivalence supervision strategy for MLLMs, encouraging alignment between feature pairs corresponding to the same 3D location across different views (positive pairs) while discouraging similarity among unrelated pairs (negative pairs). While this approach results in some performance gains, the supervision provided by such handcrafted, single-task objectives is inherently limited for 3D learning.

In contrast, recent 3D foundation models such as VGGT [37] and FLARE [44] are pretrained end-to-end on multi-view image sequences spanning a diverse set of 3D geometric tasks—including not only correspondence learning, but also depth estimation and camera parameter prediction. This comprehensive pretraining enables them to encode rich 3D properties within their features. Building on this, we propose a framework, 3DRS, that leverages these pretrained models by using their features as alignment targets for the visual outputs of MLLMs, thereby facilitating more effective 3D-aware representation learning. Unlike previous 3D MLLM approaches, in addition to traditional text token supervision, our framework employs explicit 3D-specific supervision directly on scene visual tokens. As demonstrated in our experiments (see Fig. 1), incorporating this form of 3D supervision consistently improves performance across a range of MLLMs and benchmarks. Notably, our approach incurs no additional training overhead, since the supervisory features can be pre-extracted offline.

We believe this design offers valuable new insights for applying 3D foundation models in scene understanding. The key contribution of this paper can be summarized as follows:

- We conduct a systematic evaluation of the 3D-awareness of MLLMs using multi-view correspondence metrics, and observe a strong positive correlation between 3D-aware representation quality and downstream scene understanding performance across diverse tasks, datasets, and models.
- We propose a 3D-aware representation supervision framework that aligns MLLM visual features with those of a 3D geometry-pretrained model, enabling effective 3D feature learning.
- Extensive experiments demonstrate consistent performance improvements across multiple MLLMs and 3D scene understanding benchmarks, validating the effectiveness and generality of our approach.

2 Method

2.1 Investigating 3D-Aware Representation Learning in MLLMs

2.1.1 Preliminaries

A MLLM typically consists of two main components: an image encoder $\mathcal{E}_{\text{img}}$ and a text decoder $\mathcal{T}$. In this work, the input to our MLLM comprises a set of N multi-view images $\mathcal{I} = \{I_1, I_2, \ldots, I_N\}$, each associated with per-pixel 3D coordinates $\mathcal{C} = \{\mathbf{C}_1, \mathbf{C}_2, \ldots, \mathbf{C}_N\}$, where $\mathbf{C}_i \in \mathbb{R}^{H\times W\times 3}$ for image I_i of size $H \times W$. The 3D coordinates for each pixel are computed from the depth map and the corresponding camera intrinsic and extrinsic parameters; detailed formulas and procedures can be found in the App. A.1.

The MLLM receives both multi-view images and language instructions as input. Internally, for each image I_i, the image encoder $\mathcal{E}_{\text{img}}$ extracts visual features $\mathbf{F}_i \in \mathbb{R}^{H\times W\times d}$, where d is the feature dimension. Following Video3DLLM [48], we encode the per-pixel 3D coordinates via a positional encoding function $\phi(\cdot)$ and inject this information into the image features by addition:

$$\mathbf{F}_i^{3D} = \mathbf{F}_i + \phi(\mathbf{C}_i).$$

This design allows the MLLM to inherit 2D perceptual knowledge from pretraining while equipping it with explicit 3D priors.

During finetuning, the MLLM—which we denote as f_θ—passes visual features $\{\mathbf{F}_i^{3D}\}_{i=1}^N$ with the instruction tokens to the text decoder for autoregressive text generation. After the processing of the text decoder, we refer to the final per-pixel visual embedding of pixel p in image I_i from LLM as $\mathbf{f}_i(p)$. The model is optimized by minimizing the standard cross-entropy loss:

$$\mathcal{L}_{\text{CE}} = -\sum_{t=1}^{T} \log p_\theta(y_t \mid y_{<t}, \{I_i, \mathbf{C}_i\}_{i=1}^N, \text{instruction}),$$

where y_t is the t-th output token, and p_θ is the probability predicted by the model given all previous tokens and the multimodal context (i.e., images and instructions).

2.1.2 Assessing 3D Feature Learning via Multi-View Correspondence

Inspired by the fact that cross-view correspondences are of crucial importance for 3D modeling [17], we propose to use a correspondence-based evaluation framework. Given that the input consists of multi-view images, a natural metric for 3D feature quality is the strength of correspondence across views for the same 3D spatial location. This requires the model to associate and align objects or regions that occupy the same position in 3D space, regardless of viewpoint.

Voxelization and correspondence pair construction. We first voxelize the 3D scene into a regular grid of voxels $\mathcal{V} = \{v_1, \ldots, v_M\}$. For each view I_i, given its per-pixel 3D coordinates $\mathbf{C}_i$, we assign every pixel's feature $\mathbf{f}_i(p)$ to a voxel according to its 3D position. Features from different views that fall into the same voxel v_k are regarded as *correspondence pairs*.

Feature similarity and correspondence scores. Let $\mathcal{P}_k$ denote all correspondence feature pairs in voxel v_k, i.e., all pairs $(\mathbf{f}_i(p), \mathbf{f}_j(q))$ where both pixels p and q from images I_i and I_j are assigned to v_k with $i \neq j$. For any pair of visual features $(\mathbf{f}_a, \mathbf{f}_b)$ from the last layer of MLLM, feature similarity is measured by the cosine similarity:

$$S(\mathbf{f}_a, \mathbf{f}_b) = \frac{\mathbf{f}_a^\top \mathbf{f}_b}{\|\mathbf{f}_a\| \cdot \|\mathbf{f}_b\|}.$$

For each sequence, we compute:

$$\bar{S} = \frac{1}{|\mathcal{P}|} \sum_{(\mathbf{f}_a, \mathbf{f}_b) \in \mathcal{P}} S(\mathbf{f}_a, \mathbf{f}_b),$$

where $\bar{S}$ and $\mathcal{P}$ denote the *correspondence score* for each sequence and all the correspondence pairs in this sequence. A higher correspondence score indicates that the model produces more consistent features across views for the same 3D spatial location, reflecting stronger 3D-aware representation learning.

2.1.3 Quality of 3D Feature vs. Downstream Task Performance.

We evaluate three representative MLLMs, LLaVA-Next-Video, LLaVA-OneVision, and Qwen2-VL, on five diverse 3D scene understanding benchmarks, including visual grounding (Multi3DRefer, ScanRefer), captioning (Scan2Cap), and question answering (ScanQA, SQA3D). All benchmarks are based on multi-view RGBD sequences. The three MLLMs respectively emphasize video understanding, joint image-video reasoning, and advanced arbitrary-resolution visual encoding.

To analyze the relationship between 3D feature learning and downstream task performance, we sort samples within each dataset by their correspondence scores and divide them into four quartiles (Q1–Q4, lowest to highest). From Fig. 2, we observe a clear trend: *as the correspondence score increases, the model's performance on the downstream task consistently improves.* This strong positive correlation demonstrates the critical importance of 3D-aware representation quality for effective scene understanding in MLLMs.

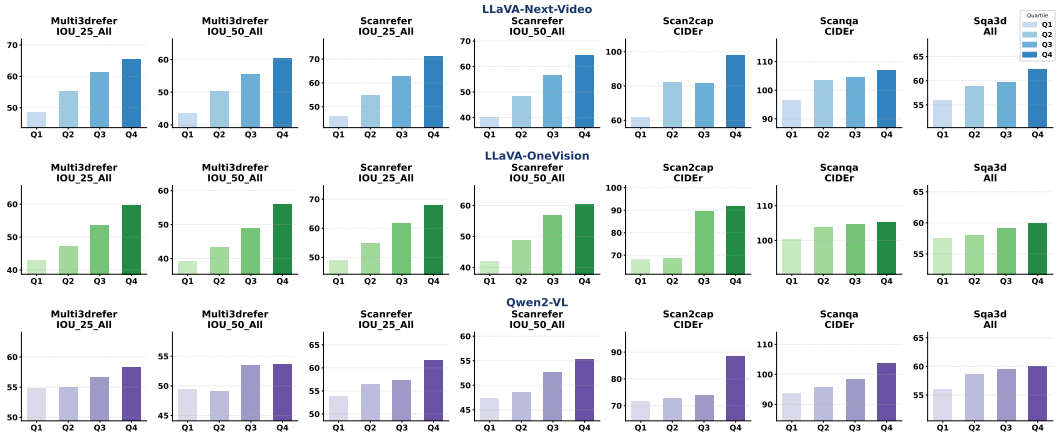

Figure 2: **Performance across correspondence score quartiles.** Model performance across correspondence score quartiles (Q1–Q4, lowest to highest) for each dataset. Samples were divided into quartiles by their correspondence scores. A clear trend is observed: model accuracy improves as the correspondence score increases.

These findings highlight the need for strategies to further enhance 3D-aware representation learning in MLLMs, which we address in the next section.

2.2 Enhancing 3D-Aware Representation Learning in MLLMs

2.2.1 Correspondence-based 3D Supervision Loss

Inspired by our correspondence-based evaluation, a straightforward approach is to directly supervise the MLLM's visual features to be consistent for matched 3D locations across views and dissimilar

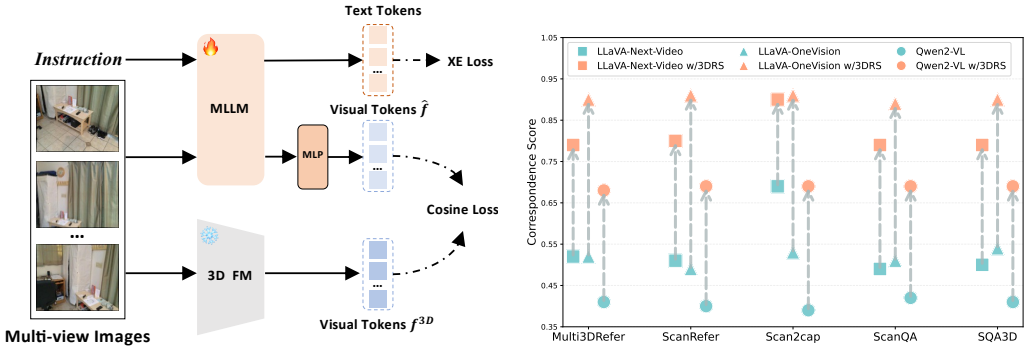

(a) **Details of 3DRS.** (b) **Comparison of correspondence learning.**

Figure 3: (a) 3DRS uses a 3D foundation model to supervise the visual representation of the MLLM. (b) 3DRS effectively improves the correspondence learning for MLLMs.

for mismatched locations. We let $\mathcal{P}_k^+$ denote all positive feature pairs in voxel v_k, i.e., all pairs $(\mathbf{f}_i(p), \mathbf{f}_j(q))$ where pixels p and q from images I_i and I_j are assigned to v_k with $i \neq j$. Similarly, $\mathcal{P}_k^-$ denotes negative pairs between v_k and any other voxel v_l ($l \neq k$). We supervise these objectives directly using a simple loss function by maximizing the feature similarity in $\mathcal{P}^+$ and minimizing that in $\mathcal{P}^-$:

$$\mathcal{L}_{\text{corr}}^{+} = \frac{1}{|\mathcal{P}^{+}|} \sum_{(\mathbf{f}_a, \mathbf{f}_b) \in \mathcal{P}^{+}} \left[1 - S(\mathbf{f}_a, \mathbf{f}_b)\right],$$

$$\mathcal{L}_{\text{corr}}^{-} = \frac{1}{|\mathcal{P}^{-}|} \sum_{(\mathbf{f}_a, \mathbf{f}_b) \in \mathcal{P}^{-}} S(\mathbf{f}_a, \mathbf{f}_b).$$

The overall correspondence loss is a weighted sum:

$$\mathcal{L}_{\text{corr}} = \mathcal{L}_{\text{corr}}^{+} + \mathcal{L}_{\text{corr}}^{-}.$$

By directly supervising positive pairs to be similar and negative pairs to be dissimilar, this correspondence loss encourages the model to learn multi-view 3D correspondences, thus enhancing the 3D-awareness of the learned representations. As will be shown in the experiments Sec. 3, supplementing the standard cross-entropy objective with $\mathcal{L}_{\text{corr}}$ leads to improvements in downstream task performance. However, as this loss primarily targets view equivariance, the range of 3D properties captured remains limited, motivating the need for richer supervision.

2.2.2 3D Foundation Model-Guided Feature Distillation

To overcome the inherent limitations of single-task supervision, we further introduce a knowledge distillation framework, 3DRS, that leverages the rich 3D priors embedded in 3D foundation models, e.g, FLARE and VGGT. These models are pretrained on a wide array of 3D geometric tasks—including correspondence learning, camera parameter estimation, multi-view depth prediction, and dense point cloud reconstruction—which enables them to extract robust and highly 3D-aware visual features from multi-view image sequences.

Distillation target preparation. As shown in Fig. 3a, given a set of multi-view images $\mathcal{I}$ for a scene, we first input them into a pretrained 3D foundation model g, which outputs a collection of per-pixel visual features $\{\mathbf{f}_i^{\text{3D}}(p)\}$ for each image I_i and pixel p. Since the spatial resolution of these features may differ from those of the MLLM outputs $\{\mathbf{f}_i(p)\}$, we apply 2D average pooling to the 3D foundation model's output to match the MLLM feature map size.

Feature alignment and loss. To align the MLLM's per-pixel visual features with the 3D foundation model, we first process each $\mathbf{f}_i(p)$ with a two-layer MLP (denoted as $\text{MLP}_{\text{align}}$) to ensure

compatibility in feature dimension:

$$\hat{\mathbf{f}}_i(p) = \mathrm{MLP}_{\mathrm{align}}(\mathbf{f}_i(p)).$$

We then employ a cosine similarity-based distillation loss to maximize the alignment between the MLLM features $\hat{\mathbf{f}}_i(p)$ and the corresponding 3D foundation model features $\mathbf{f}_i^{\mathrm{3D}}(p)$:

$$\mathcal{L}_{\mathrm{align}} = -\frac{1}{NHW} \sum_{i=1}^{N} \sum_{p \in I_i} S\left(\hat{\mathbf{f}}_i(p), \mathbf{f}_i^{\mathrm{3D}}(p)\right),$$

where $S(\cdot, \cdot)$ denotes cosine similarity, and the sum is calculated over all pixels and views in the batch.

Overall training objective. The final training objective for the MLLM combines the standard cross-entropy loss for text generation and the 3D foundation model distillation loss:

$$\mathcal{L}_{\mathrm{total}} = \mathcal{L}_{\mathrm{CE}} + \mathcal{L}_{\mathrm{align}}.$$

This approach enables the MLLM to inherit comprehensive 3D knowledge from powerful geometry-pretrained models, facilitating the learning of richer and more robust 3D-aware representations. Importantly, the distillation targets from the 3D foundation model can be precomputed offline, introducing no additional overhead during MLLM fine-tuning.

As illustrated in Fig. 3b, we compare the correspondence scores before and after applying our 3DRS, where VGGT serves as the foundation model. The results consistently demonstrate that introducing 3DRS leads to substantial improvements in correspondence learning ability across all evaluated MLLMs and benchmarks. This proves the effectiveness of leveraging a pretrained 3D foundation model as a teacher model for enhancing 3D-aware representation learning in MLLMs. More comprehensive experimental results and analyses are detailed in Sec. 3.

3 Experiments

3.1 Datasets and Evaluation Metrics

Datasets. We evaluate our approach on five benchmarks that collectively span key challenges in 3D scene understanding. ScanRefer [4] focuses on localizing objects using free-form language, while Multi3DRefer [45] generalizes this to queries referencing zero, one, or multiple objects, better reflecting real-world ambiguity. Scan2Cap [9] addresses dense captioning by pairing detected objects in 3D scans with natural language descriptions. For question answering, ScanQA [2] tasks models with answering open-ended questions grounded in 3D geometry and semantics, and SQA3D [27] goes further by requiring situated reasoning: agents must interpret their position and context to answer complex queries. All datasets are sourced from the richly annotated ScanNet [10] corpus, and we follow standard validation and test splits as established in prior work [20, 50, 8, 48]. The statistics of training sets are detailed in the App. A.2.

Evaluation metrics. For ScanRefer, we report accuracy at IoU thresholds of 0.25 and 0.5 (Acc@0.25, Acc@0.5). Multi3DRefer uses F1 scores at matching IoU thresholds. Scan2Cap is evaluated by CIDEr and BLEU-4 scores at 0.5 IoU (C@0.5, B-4@0.5). ScanQA is assessed by CIDEr and exact match accuracy (C, EM), while SQA3D uses exact match accuracy as the metric.

3.2 Implementation Details

Our experiments leverage several MLLMs, including LLaVA-Next-Video 7B [46], LLaVA-OneVision 7B [23], and Qwen2-VL 7B [38]. In addition to these baselines, we systematically compare the effect of using 2D versus 3D foundation models as teachers for MLLM finetuning. The 2D teacher models include DINOv2 [30], MAE [18], and SigLIP [36], while the 3D teacher models comprise FLARE [44] and VGGT [37]. Unless stated otherwise, we use LLaVA-Next-Video as the MLLM and VGGT as the representation teacher for our experiments.

For both training and inference, we uniformly sample 32 frames per scan to construct multi-view image sets. For evaluating the correspondence score, we use the voxel size of 0.1 for voxelization.

Table 1: Performance comparison on 3D scene understanding benchmarks. Specialists are single-task methods, while generalists target multiple tasks. Bold denotes best performance.

Method	ScanRefer		Multi3DRefer		Scan2Cap		ScanQA		SQA3D
	Acc@0.25	Acc@0.5	F1@0.25	F1@0.5	C@0.5	B-4@0.5	C	EM	EM
Specialists									
ScanRefer [4]	37.3	24.3	–	–	–	–	–	–	–
MVT [22]	40.8	33.3	–	–	–	–	–	–	–
3DVG-Trans [47]	45.9	34.5	–	–	–	–	–	–	–
ViL3DRel [6]	47.9	37.7	–	–	–	–	–	–	–
M3DRef-CLIP [45]	51.9	44.7	42.8	–	38.4	–	–	–	–
Scan2Cap [9]	–	–	–	–	35.2	22.4	–	–	–
ScanQA [2]	–	–	–	–	–	–	64.9	21.1	47.2
3D-VisTA [51]	50.6	45.8	–	–	66.9	34.0	69.6	22.4	48.5
Generalists									
3D-LLM(Flamingo) [19]	21.2	–	–	–	–	–	59.2	20.4	–
3D-LLM(BLIP2-flant5) [19]	30.3	–	–	–	–	–	69.4	20.5	–
Chat-3D [39]	–	–	–	–	–	–	53.2	–	–
Chat-3D v2 [20]	42.5	38.4	45.1	41.6	63.9	31.8	87.6	–	54.7
LL3DA [7]	–	–	–	–	62.9	36.0	76.8	–	–
SceneLLM [13]	–	–	–	–	–	–	80.0	27.2	53.6
LEO [21]	–	–	–	–	72.4	38.2	101.4	21.5	50.0
Grounded 3D-LLM [8]	47.9	44.1	45.2	40.6	70.6	35.5	72.7	–	–
PQ3D [52]	57.0	51.2	–	50.1	80.3	36.0	–	–	47.1
ChatScene [20]	55.5	50.2	57.1	52.4	77.1	36.3	87.7	21.6	54.6
LLaVA-3D [50]	54.1	42.4	–	–	79.2	41.1	91.7	27.0	55.6
Inst3D-LLM [43]	57.8	51.6	58.3	53.5	79.7	38.3	88.6	24.6	–
3D-LLaVA [11]	51.2	40.6	–	–	78.8	36.9	92.6	–	54.5
Video-3D LLM [48]	58.1	51.7	58.0	52.7	83.8	41.3	102.1	30.1	58.6
3DRS	**62.9**	**56.1**	**60.4**	**54.9**	**86.1**	**41.6**	**104.8**	**30.3**	**60.6**

All models are optimized using Adam, with a batch size of 16 and a warm-up ratio of 0.03. The learning rates are set to a maximum of 1×10^{-5} for the language model and 2×10^{-6} for the visual backbone during the warm-up period. During training for visual grounding and dense captioning, ground truth object regions are used as candidates, whereas during inference, we follow the procedure of [20, 21, 48] and employ Mask3D [33] to generate object proposals. For LLaVA-Next-Video and LLaVA-OneVision, we finetune all model parameters. For Qwen2-VL, due to GPU memory constraints, we finetune only the projector and the LLM components. We use 8 H100 NVIDIA GPUs for all experiments.

3.3 Comparison with State-of-the-Art Models

Table 1 presents a comprehensive comparison between our approach, task-specific specialist models—which require fine-tuning on individual datasets—and 3D generalist models that are capable of handling multiple tasks. Compared to specialist models, our approach achieves substantial performance improvements. This demonstrates the significant benefits brought by joint training and the LLM-based architecture, which contribute to superior generalization and feature integration compared to methods tailored for specific tasks.

Furthermore, our method consistently outperforms 3D generalist approaches that utilize point clouds as input, such as LL3DA, Chat-3D, Grounded 3D-LLM, and 3D-LLaVA. Compared to Inst3D-LLM—which fuses multi-view images and point clouds—our approach also shows clear advantages, highlighting the strength of leveraging MLLMs as the backbone. Additionally, our method achieves considerable improvements over other MLLM-based methods, including LLaVA-3D and Video-3D LLM. These results collectively indicate that enhancing the 3D-awareness of MLLMs is highly effective for 3D scene understanding tasks, further validating the effectiveness of our proposed strategy.

3.4 Diagnostic Study

Effectiveness with different MLLMs. Table 2 demonstrates that integrating 3DRS with different MLLMs—LLaVA-Next-Video, LLaVA-OneVision, and Qwen2-VL—consistently boosts performance across all evaluated benchmarks. For example, LLaVA-Next-Video w/ 3DRS improves

Table 2: Performance comparison of 3DRS when using with different MLLMs.

Method	ScanRefer		Multi3DRef		Scan2Cap		ScanQA		SQA3D
	Acc@0.25	Acc@0.5	F1@0.25	F1@0.5	B-4@0.5	C@0.5	C	EM	EM
LLaVA-Next-Video [46]	58.1	51.7	58.0	52.7	41.3	83.8	102.1	30.1	58.6
LLaVA-Next-Video w/ 3DRS	**62.9**	**56.1**	**60.4**	**54.9**	**41.6**	**86.1**	**104.8**	**30.3**	**60.6**
LLaVA-OneVision [23]	57.3	51.0	57.1	51.9	40.4	81.7	101.7	29.0	57.4
LLaVA-OneVision w/ 3DRS	**61.8**	**55.0**	**60.5**	**55.0**	**41.2**	**83.1**	**104.0**	**29.5**	**59.4**
Qwen2-VL [38]	57.0	50.8	56.2	51.4	39.5	79.4	97.5	28.7	58.6
Qwen2-VL w/ 3DRS	**60.1**	**53.5**	**58.5**	**54.5**	**40.9**	**81.6**	**99.2**	**28.9**	**60.0**

ScanRefer Acc@0.25 from 58.1 to 62.9, and Multi3DRef F1@0.25 from 58.0 to 60.4. Similar gains are observed for LLaVA-OneVision and Qwen2-VL, where 3DRS brings improvements on every dataset and metric. These results highlight the general applicability of our approach and its effectiveness in enhancing 3D scene understanding for various MLLMs.

Comparison between 2D and 3D foundation models. Table 3 compares the performance of using 2D and 3D foundation models as representation supervisors. It is clear that 3D foundation models (FLARE and VGGT) outperform all 2D foundation models (MAE, Siglip2, Dinov2) across almost every metric. This performance gap can be attributed to the inherent difference in the prior knowledge captured by 2D and 3D foundation models. 3D models are pre-trained on large-scale 3D data and thus better capture geometric structure, spatial relationships, and depth information, which are critical for 3D scene understanding tasks. In contrast, 2D foundation models, trained on images, lack explicit 3D spatial priors and struggle to provide effective supervision for learning 3D-aware representations. This highlights the importance of 3D-specific foundation models for achieving strong results in downstream 3D tasks.

Comparison of supervision signal. Table 4 shows that using correspondence loss for supervision brings improvements over the baseline, demonstrating the effectiveness of encouraging the model to learn multi-view correspondences. However, when 3D foundation model supervision is applied, the performance increases even further across all metrics. This indicates that 3D foundation models, with their rich 3D prior knowledge learned during pre-training, can more effectively enhance the 3D representation ability of MLLMs and yield greater gains for 3D understanding tasks.

Comparison of supervision at different layers. Table 5 examines the effect of applying 3D foundation model supervision at different layers of the network. The results reveal that supervision at deeper layers, especially the last layer, leads to the highest performance. This is likely because deeper layers are closer to the output and thus have a more direct impact on the final predictions. Additionally, these layers possess more parameters and a greater capacity to fit 3D features, which results in larger improvements on downstream tasks.

Table 3: Ablation study on using different 2D/3D foundation models as the representation supervisor. Bold denotes the best in each group.

Representation Supervisor	ScanRefer		Multi3DRef		Scan2Cap		ScanQA		SQA3D
	Acc@0.25	Acc@0.5	F1@0.25	F1@0.5	C@0.5	B-4@0.5	C	EM	EM
Baseline	58.1	51.7	58.0	52.7	83.8	41.3	102.1	30.1	58.6
2D Foundation Models									
Siglip2 [36]	58.2	52.9	59.7	53.1	81.7	40.2	100.2	29.1	59.4
MAE [18]	59.1	**53.7**	**60.0**	**53.7**	**82.8**	**40.4**	102.5	29.5	59.2
Dinov2 [30]	**59.8**	53.3	58.5	53.5	80.3	39.3	**103.5**	**29.6**	**60.1**
3D Foundation Models									
FLARE [44]	62.1	55.7	59.8	54.8	**86.6**	**42.5**	104.4	30.1	60.1
VGGT [37]	**62.9**	**56.1**	**60.4**	**54.9**	86.1	41.6	**104.8**	**30.3**	**60.6**

Visualizations Fig. 4 illustrates qualitative results of our method across three tasks: visual grounding, object captioning, and question answering.

Table 4: Comparison of different supervision strategies.

Method	Multi3DRef		ScanRefer	
	Acc@0.25	Acc@0.5	F1@0.25	F1@0.5
Baseline	58.0	52.7	58.1	51.7
w/ Correspondence Loss	60.1	53.3	59.1	53.7
w/ 3D Supervision	**62.9**	**56.1**	**60.4**	**54.9**

Table 5: 3D foundation model supervision at different layers.

Layer	Multi3DRef		ScanRefer	
	Acc@0.25	Acc@0.5	F1@0.25	F1@0.5
Last Layer	**62.9**	**56.1**	**60.4**	**54.9**
3rd Last Layer	61.7	54.9	59.7	54.3
5th Last Layer	61.4	54.8	59.3	54.0
10th Last Layer	59.1	53.6	53.3	53.8

For the visual grounding task (top two rows), the model is required to localize objects within a 3D scene based on natural language descriptions. Each example shows the ground truth bounding box (blue), the result from a baseline method (red), and our prediction (green). In both cases, our method's predictions match the ground truth more closely than the baseline, demonstrating improved grounding accuracy.

In the object captioning task (middle two rows), the model generates descriptive captions for specific objects in the scene. The captions from the ground truth, the baseline, and our method are shown alongside their corresponding regions. We also report CIDEr scores to measure caption quality. Our approach produces more accurate and detailed descriptions with significantly higher CIDEr scores compared to the baseline.

For the question answering task (bottom two rows), the model answers questions about the scene. Ground truth answers, baseline outputs, and our results are provided for each question. Red rectangles highlight the visual evidence used by our model to generate the answers. Our method provides correct answers that align with the ground truth, whereas the baseline often fails to do so.

Overall, the visualizations demonstrate that our approach consistently outperforms the baseline across all tasks, delivering more accurate grounding, richer object descriptions, and more reliable answers to visual questions.

4 Related Work

4.1 Scene Understanding with Large Language Models

LLMs, owing to their strong reasoning capabilities and remarkable success in 2D image understanding, have been widely applied to scene understanding tasks. Early works such as PointLLM [40], Point-Bind [16], GPT4Point [31], MiniGPT-3D [34], and Chat-3D [39] leverage the alignment between point cloud and text features to facilitate 3D scene comprehension. Building on this foundation, methods like Grounded 3D-LLM [8], LL3DA [7], 3D-LLaVA [11], and Inst3D-LLM [43] design more advanced cross-modal modules to better fuse multi-modal features, thereby enhancing scene representations. Furthermore, Chat-Scene [20] and Inst3D-LLM [43] exploit the complementary nature of 2D and 3D features to further boost scene understanding.

Some recent approaches, such as 3D-LLM [19] and Scene LLM [13], employ multi-view inputs and introduce 3D priors to transform 2D representations into a 3D-aware format. Thanks to pre-training on large-scale image-text datasets, methods based on MLLMs are gaining increasing popularity in the field of scene understanding. For instance, LLaVA-3D [50] takes multi-view images as input and utilizes voxelization to reduce the dimensionality of representations, thus lowering computational costs while leveraging the strengths of MLLMs. However, many MLLMs require specially structured inputs, making them incompatible with certain approaches. Video 3D-LLM [48] and GPT4Scene [32] more naturally inherit the MLLM pipeline by introducing 3D priors—such as positional embeddings or spatial markers—enabling the model to better comprehend 3D scene content.

Our work follows this line of MLLM-based scene understanding, aiming to probe the 3D-awareness of MLLMs and analyze their relationships with downstream tasks. In particular, we demonstrate that introducing guidance from 3D foundation models can effectively enhance the representational capability of MLLMs for 3D scene understanding.

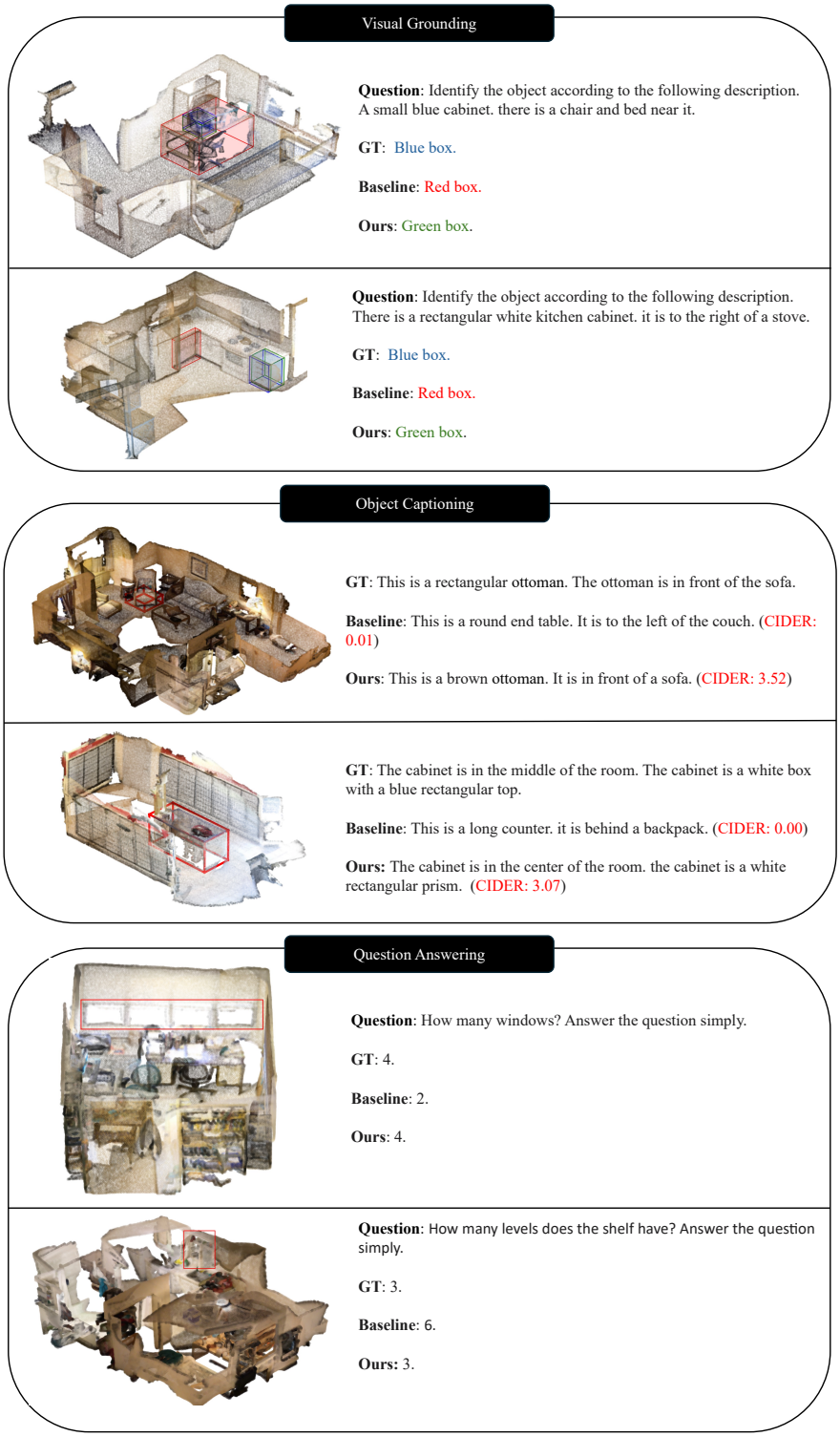

Figure 4: **Visualization of Results Across Different Tasks.** (a) Visual Grounding: The predicted bounding box closely aligns with the ground truth. (b) Object Captioning: Our method generates accurate captions for each referred object. (c) Question Answering: The model provides precise answers, where we use the red rectangles to indicate the visual cues utilized for each response. Best viewed when zoomed in.

4.2 3D-Awareness Study in Visual Models

Several studies have explored 3D-awareness; however, most of this research has focused on pure vision models rather than MLLMs, and primarily on 2D foundation models instead of 3D ones. For example, Probe3D [12] and Lexicon3D [28] conduct empirical analyses of the 3D-awareness in visual foundation models. CUA-O3D [24] proposes integrating multiple 2D foundation models for 3D scene understanding, while Yang et al. [42] evaluates and enhances the 3D-awareness of ViT-based models for various downstream tasks.

In contrast to these works, our study centers on the 3D-awareness of MLLMs. Instead of enhancing 3D feature learning with 2D foundation models, we introduce 3D foundation models as supervisors to directly guide and improve the 3D representation ability of MLLMs.

5 Conclusion

In this paper, we systematically investigate the 3D representation capabilities of MLLMs for scene understanding. While previous studies have primarily focused on the impact of 2D foundation models, our work is the first to explore the value of 3D foundation models in this setting. Specifically, we introduce 3DRS, a framework that delivers direct 3D-aware supervision to MLLMs via pretrained 3D foundation models. Extensive experiments show that our approach consistently enhances performance across a range of 3D scene understanding tasks, underscoring the importance and potential of 3D foundation models for multimodal scene understanding.

References

[1] Rohan Anil, Sebastian Borgeaud, Yonghui Wu, Jean-Baptiste Alayrac, Jiahui Yu, Radu Soricut, Johan Schalkwyk, Andrew M Dai, Anja Hauth, Katie Millican, et al. Gemini: A family of highly capable multimodal models. corr, abs/2312.11805, 2023. doi: 10.48550. *Arxiv e-prints*.

[2] Daichi Azuma, Taiki Miyanishi, Shuhei Kurita, and Motoaki Kawanabe. Scanqa: 3d question answering for spatial scene understanding. In *CVPR*, 2022. License: Creative Commons Attribution-NonCommercial-ShareAlike 3.0 Unported License.

[3] Daigang Cai, Lichen Zhao, Jing Zhang, Lu Sheng, and Dong Xu. 3djcg: A unified framework for joint dense captioning and visual grounding on 3d point clouds. In *CVPR*, 2022.

[4] Dave Zhenyu Chen, Angel X Chang, and Matthias Nießner. Scanrefer: 3d object localization in rgb-d scans using natural language. In *European conference on computer vision*, 2020. License: Creative Commons Attribution-NonCommercial-ShareAlike 3.0 Unported License.

[5] Dave Zhenyu Chen, Qirui Wu, Matthias Nießner, and Angel X. Chang. D^3net: A unified speaker-listener architecture for 3d dense captioning and visual grounding. In *ECCV*, volume 13692, 2022.

[6] Shizhe Chen, Pierre-Louis Guhur, Makarand Tapaswi, Cordelia Schmid, and Ivan Laptev. Language conditioned spatial relation reasoning for 3d object grounding. In *NeurIPS*, 2022.

[7] Sijin Chen, Xin Chen, Chi Zhang, Mingsheng Li, Gang Yu, Hao Fei, Hongyuan Zhu, Jiayuan Fan, and Tao Chen. LL3DA: visual interactive instruction tuning for omni-3d understanding, reasoning, and planning. In *CVPR*, 2024.

[8] Yilun Chen, Shuai Yang, Haifeng Huang, Tai Wang, Ruiyuan Lyu, Runsen Xu, Dahua Lin, and Jiangmiao Pang. Grounded 3d-llm with referent tokens. *Arxiv e-prints*, 2024.

[9] Zhenyu Chen, Ali Gholami, Matthias Nießner, and Angel X Chang. Scan2cap: Context-aware dense captioning in rgb-d scans. In *CVPR*, 2021. License: Creative Commons Attribution-NonCommercial-ShareAlike 3.0 Unported License.

[10] Angela Dai, Angel X Chang, Manolis Savva, Maciej Halber, Thomas Funkhouser, and Matthias Nießner. Scannet: Richly-annotated 3d reconstructions of indoor scenes. In *CVPR*, 2017. License: ScanNet Terms of Use.

[11] Jiajun Deng, Tianyu He, Li Jiang, Tianyu Wang, Feras Dayoub, and Ian Reid. 3d-llava: Towards generalist 3d lmms with omni superpoint transformer. *Arxiv e-prints*, 2025.

[12] Mohamed El Banani, Amit Raj, Kevis-Kokitsi Maninis, Abhishek Kar, Yuanzhen Li, Michael Rubinstein, Deqing Sun, Leonidas Guibas, Justin Johnson, and Varun Jampani. Probing the 3d awareness of visual foundation models. In *CVPR*, 2024.

[13] Rao Fu, Jingyu Liu, Xilun Chen, Yixin Nie, and Wenhan Xiong. Scene-llm: Extending language model for 3d visual understanding and reasoning. *Arxiv e-prints*, 2024.

[14] Aaron Grattafiori, Abhimanyu Dubey, Abhinav Jauhri, Abhinav Pandey, Abhishek Kadian, Ahmad Al-Dahle, Aiesha Letman, Akhil Mathur, Alan Schelten, Alex Vaughan, et al. The llama 3 herd of models. *Arxiv e-prints*, 2024.

[15] Daya Guo, Dejian Yang, Haowei Zhang, Junxiao Song, Ruoyu Zhang, Runxin Xu, Qihao Zhu, Shirong Ma, Peiyi Wang, Xiao Bi, et al. Deepseek-r1: Incentivizing reasoning capability in llms via reinforcement learning. 2025.

[16] Ziyu Guo, Renrui Zhang, Xiangyang Zhu, Yiwen Tang, Xianzheng Ma, Jiaming Han, Kexin Chen, Peng Gao, Xianzhi Li, Hongsheng Li, et al. Point-bind & point-llm: Aligning point cloud with multi-modality for 3d understanding, generation, and instruction following. *Arxiv e-prints*, 2023.

[17] Richard Hartley. *Multiple view geometry in computer vision*, volume 665. Cambridge university press, 2003.

[18] Kaiming He, Xinlei Chen, Saining Xie, Yanghao Li, Piotr Dollár, and Ross Girshick. Masked autoencoders are scalable vision learners. In *CVPR*, 2022.

[19] Yining Hong, Haoyu Zhen, Peihao Chen, Shuhong Zheng, Yilun Du, Zhenfang Chen, and Chuang Gan. 3d-llm: Injecting the 3d world into large language models. In *NeurIPS*, 2023.

[20] Haifeng Huang, Zehan Wang, Rongjie Huang, Luping Liu, Xize Cheng, Yang Zhao, Tao Jin, and Zhou Zhao. Chat-3d v2: Bridging 3d scene and large language models with object identifiers. *Arxiv e-prints*, 2023.

[21] Jiangyong Huang, Silong Yong, Xiaojian Ma, Xiongkun Linghu, Puhao Li, Yan Wang, Qing Li, Song-Chun Zhu, Baoxiong Jia, and Siyuan Huang. An embodied generalist agent in 3d world. In *ICML*, 2024.

[22] Shijia Huang, Yilun Chen, Jiaya Jia, and Liwei Wang. Multi-view transformer for 3d visual grounding. In *CVPR*, 2022.

[23] Bo Li, Yuanhan Zhang, Dong Guo, Renrui Zhang, Feng Li, Hao Zhang, Kaichen Zhang, Yanwei Li, Ziwei Liu, and Chunyuan Li. Llava-onevision: Easy visual task transfer. *Arxiv e-prints*, 2024.

[24] Jinlong Li, Cristiano Saltori, Fabio Poiesi, and Nicu Sebe. Cross-modal and uncertainty-aware agglomeration for open-vocabulary 3d scene understanding. 2025.

[25] Haotian Liu, Chunyuan Li, Qingyang Wu, and Yong Jae Lee. Visual instruction tuning. *NeurIPS*, 2023.

[26] Zuyan Liu, Yuhao Dong, Ziwei Liu, Winston Hu, Jiwen Lu, and Yongming Rao. Oryx MLLM: on-demand spatial-temporal understanding at arbitrary resolution. *Arxiv e-prints*, 2024.

[27] Xiaojian Ma, Silong Yong, Zilong Zheng, Qing Li, Yitao Liang, Song-Chun Zhu, and Siyuan Huang. SQA3D: situated question answering in 3d scenes. In *ICLR*, 2023. License: CC-BY-4.0.

[28] Yunze Man, Shuhong Zheng, Zhipeng Bao, Martial Hebert, Liangyan Gui, and Yu-Xiong Wang. Lexicon3d: Probing visual foundation models for complex 3d scene understanding. *NeurIPS*, 2024.

[29] OpenAI. GPT-4 technical report. *Arxiv e-prints*, 2023.

[30] Maxime Oquab, Timothée Darcet, Théo Moutakanni, Huy Vo, Marc Szafraniec, Vasil Khalidov, Pierre Fernandez, Daniel Haziza, Francisco Massa, Alaaeldin El-Nouby, et al. Dinov2: Learning robust visual features without supervision. *Arxiv e-prints*, 2023.

[31] Zhangyang Qi, Ye Fang, Zeyi Sun, Xiaoyang Wu, Tong Wu, Jiaqi Wang, Dahua Lin, and Hengshuang Zhao. Gpt4point: A unified framework for point-language understanding and generation. In *CVPR*, 2024.

[32] Zhangyang Qi, Zhixiong Zhang, Ye Fang, Jiaqi Wang, and Hengshuang Zhao. Gpt4scene: Understand 3d scenes from videos with vision-language models. *Arxiv e-prints*, 2025.

[33] Jonas Schult, Francis Engelmann, Alexander Hermans, Or Litany, Siyu Tang, and Bastian Leibe. Mask3d: Mask transformer for 3d semantic instance segmentation. In *International Conference on Robotics and Automation*, 2023.

[34] Yuan Tang, Xu Han, Xianzhi Li, Qiao Yu, Yixue Hao, Long Hu, and Min Chen. Minigpt-3d: Efficiently aligning 3d point clouds with large language models using 2d priors. In *ACM Multi*, 2024.

[35] Yuan Tang, Xu Han, Xianzhi Li, Qiao Yu, Jinfeng Xu, Yixue Hao, Long Hu, and Min Chen. More text, less point: Towards 3d data-efficient point-language understanding. In *AAAI*, 2025.

[36] Michael Tschannen, Alexey Gritsenko, Xiao Wang, Muhammad Ferjad Naeem, Ibrahim Alabdulmohsin, Nikhil Parthasarathy, Talfan Evans, Lucas Beyer, Ye Xia, Basil Mustafa, et al. Siglip 2: Multilingual vision-language encoders with improved semantic understanding, localization, and dense features. *Arxiv e-prints*, 2025.

[37] Jianyuan Wang, Minghao Chen, Nikita Karaev, Andrea Vedaldi, Christian Rupprecht, and David Novotny. Vggt: Visual geometry grounded transformer. *Arxiv e-prints*, 2025.

[38] Peng Wang, Shuai Bai, Sinan Tan, Shijie Wang, Zhihao Fan, Jinze Bai, Keqin Chen, Xuejing Liu, Jialin Wang, Wenbin Ge, et al. Qwen2-vl: Enhancing vision-language model's perception of the world at any resolution. *Arxiv e-prints*, 2024.

[39] Zehan Wang, Haifeng Huang, Yang Zhao, Ziang Zhang, and Zhou Zhao. Chat-3d: Data-efficiently tuning large language model for universal dialogue of 3d scenes. *Arxiv e-prints*, 2023.

[40] Runsen Xu, Xiaolong Wang, Tai Wang, Yilun Chen, Jiangmiao Pang, and Dahua Lin. Pointllm: Empowering large language models to understand point clouds. In *ECCV*, 2024.

[41] An Yang, Baosong Yang, Binyuan Hui, Bo Zheng, Bowen Yu, Chang Zhou, Chengpeng Li, Chengyuan Li, et al. Qwen2 technical report. *Arxiv e-prints*, 2024.

[42] Yang You, Yixin Li, Congyue Deng, Yue Wang, and Leonidas Guibas. Multiview equivariance improves 3d correspondence understanding with minimal feature finetuning. 2024.

[43] Hanxun Yu, Wentong Li, Song Wang, Junbo Chen, and Jianke Zhu. Inst3d-lmm: Instance-aware 3d scene understanding with multi-modal instruction tuning. *Arxiv e-prints*, 2025.

[44] Shangzhan Zhang, Jianyuan Wang, Yinghao Xu, Nan Xue, Christian Rupprecht, Xiaowei Zhou, Yujun Shen, and Gordon Wetzstein. Flare: Feed-forward geometry, appearance and camera estimation from uncalibrated sparse views. *Arxiv e-prints*, 2025.

[45] Yiming Zhang, ZeMing Gong, and Angel X. Chang. Multi3drefer: Grounding text description to multiple 3d objects. In *ICCV*, 2023. License: MIT.

[46] Yuanhan Zhang, Jinming Wu, Wei Li, Bo Li, Zejun Ma, Ziwei Liu, and Chunyuan Li. Video instruction tuning with synthetic data, 2024.

[47] Lichen Zhao, Daigang Cai, Lu Sheng, and Dong Xu. 3dvg-transformer: Relation modeling for visual grounding on point clouds. In *ICCV*, 2021.

[48] Duo Zheng, Shijia Huang, and Liwei Wang. Video-3d llm: Learning position-aware video representation for 3d scene understanding. *Arxiv e-prints*, 2024.

[49] Duo Zheng, Shijia Huang, Lin Zhao, Yiwu Zhong, and Liwei Wang. Towards learning a generalist model for embodied navigation. In *CVPR*, 2024.

[50] Chenming Zhu, Tai Wang, Wenwei Zhang, Jiangmiao Pang, and Xihui Liu. Llava-3d: A simple yet effective pathway to empowering lmms with 3d-awareness. *Arxiv e-prints*, 2024.

[51] Ziyu Zhu, Xiaojian Ma, Yixin Chen, Zhidong Deng, Siyuan Huang, and Qing Li. 3d-vista: Pre-trained transformer for 3d vision and text alignment. In *ICCV*, 2023.

[52] Ziyu Zhu, Zhuofan Zhang, Xiaojian Ma, Xuesong Niu, Yixin Chen, Baoxiong Jia, Zhidong Deng, Siyuan Huang, and Qing Li. Unifying 3d vision-language understanding via promptable queries. In *ECCV*, 2024.

A Technical Appendices and Supplementary Material

A.1 World Coordinate Computation

Given a set of N images $\mathcal{I} = \{I_1, I_2, \ldots, I_N\}$, each image I_i is paired with its depth map $D_i \in \mathbb{R}^{H \times W}$, camera intrinsic matrix $K_i \in \mathbb{R}^{3\times3}$, and camera-to-world extrinsic matrix $T_i \in \mathbb{R}^{4\times4}$. For a pixel at (u, v) in image I_i, the corresponding 3D coordinate in the global coordinate system, denoted as $\mathbf{C}_i(u, v) \in \mathbb{R}^3$, is computed as:

$$\begin{bmatrix} \mathbf{C}_i(u,v) \\ 1 \end{bmatrix} = T_i \begin{bmatrix} D_i(u,v) \cdot K_i^{-1} \begin{bmatrix} u \\ v \\ 1 \end{bmatrix} \\ 1 \end{bmatrix} \tag{1}$$

Repeating this process for all pixels yields the per-pixel 3D coordinate map $\mathbf{C}_i \in \mathbb{R}^{H\times W\times3}$ for each image I_i. The complete set of coordinate maps is denoted as $\mathcal{C} = \{\mathbf{C}_1, \mathbf{C}_2, \ldots, \mathbf{C}_N\}$.

A.2 Datsests for Training

For model fine-tuning, we utilize a collection of well-established 3D vision-language datasets. Specifically, we follow the model finetuning settings of Video-3D LLM [48] by using the validation splits of ScanRefer, Multi3DRefer, Scan2Cap, and ScanQA, as well as the test split of SQA3D. Across these datasets, the number of data samples varies significantly: ScanRefer and Scan2Cap each provide 36,665 samples, while Multi3DRefer offers 43,838 entries. ScanQA contains 26,515 instances, and SQA3D is the largest with 79,445 samples. Most datasets are derived from 562 unique scans, except SQA3D, which includes 518 scans. We further report the average lengths of questions and answers for each dataset. For example, question lengths range from approximately 13 to 38 words, with Scan2Cap and ScanQA also providing answer texts, averaging 17.9 and 2.4 words in length, respectively. In SQA3D, the average question and answer lengths are 37.8 and 1.1 words.

A.3 Detailed Comparison

In this section, we provide a detailed comparison with other methods using all metrics across 5 benchmarks.

Scanrefer. Tab. 6 shows that our method 3DRS achieves the best overall performance on the ScanRefer validation set, especially in the challenging "Multiple" scenario where precise target

Table 6: Performance comparison on the validation set of ScanRefer [4]. "Unique" and "Multiple" depends on whether there are other objects of the same class as the target object.

Method	Unique		Multiple		Overall	
	Acc@0.25	Acc@0.5	Acc@0.25	Acc@0.5	Acc@0.25	Acc@0.5
ScanRefer [4]	76.3	53.5	32.7	21.1	41.2	27.4
MVT [22]	77.7	66.4	31.9	25.3	40.8	33.3
3DVG-Transformer [47]	81.9	60.6	39.3	28.4	47.6	34.7
ViL3DRel [6]	81.6	68.6	40.3	30.7	47.9	37.7
3DJCG [3]	83.5	64.3	41.4	30.8	49.6	37.3
D3Net [5]	–	72.0	–	30.1	–	37.9
M3DRef-CLIP [45]	85.3	77.2	43.8	36.8	51.9	44.7
3D-VisTA [51]	81.6	75.1	43.7	39.1	50.6	45.8
3D-LLM (Flamingo) [19]	–	–	–	–	21.2	–
3D-LLM (BLIP2-flant5) [19]	–	–	–	–	30.3	–
Grounded 3D-LLM [8]	–	–	–	–	47.9	44.1
PQ3D [52]	86.7	78.3	51.5	46.2	57.0	51.2
ChatScene [20]	89.6	82.5	47.8	42.9	55.5	50.2
LLaVA-3D [50]	–	–	–	–	54.1	42.2
Video 3D-LLM [48]	88.0	78.3	50.9	45.3	58.1	51.7
3DRS (Ours)	87.4	77.9	57.0	50.8	62.9	56.1

discrimination is required. These results demonstrate that 3DRS effectively leverages multi-view images for robust spatial understanding and accurate object localization.

Multi3DRefer. In Tab. 7, 3DRS achieves the best overall results on the Multi3DRefer validation set, with top F1 scores in both standard and challenging scenarios. Our method consistently outperforms previous approaches, especially in the difficult zero-target and distractor settings, demonstrating superior robustness and spatial understanding.

Table 7: Performance comparison on the validation set of Multi3DRefer [45]. ZT: zero-target, ST: single-target, MT: multi-target, D: distractor.

Method	ZT w/o D	ZT w/ D	ST w/o D		ST w/ D		MT		ALL	
	F1	F1	F1@0.25	F1@0.5	F1@0.25	F1@0.5	F1@0.25	F1@0.5	F1@0.25	F1@0.5
M3DRef-CLIP [45]	81.8	39.4	53.5	47.8	34.6	30.6	43.6	37.9	42.8	38.4
D3Net [5]	81.6	32.5	–	38.6	–	23.3	–	35.0	–	32.2
3DJCG [3]	94.1	66.9	–	26.0	–	16.7	–	26.2	–	26.6
Grounded 3D-LLM [8]	–	–	–	–	–	–	–	–	45.2	40.6
PQ3D [52]	85.4	57.7	–	68.5	–	43.6	–	40.9	–	50.1
ChatScene [20]	90.3	62.6	82.9	75.9	49.1	44.5	45.7	41.1	57.1	52.4
Video 3D-LLM [48]	94.7	78.5	82.6	73.4	52.1	47.2	40.8	35.7	58.0	52.7
3DRS (Ours)	95.6	79.4	79.6	71.4	57.0	51.3	43.0	37.8	60.4	54.9

ScanQA. In Tab. 8, 3DRS achieves the best performance on the ScanQA validation set across almost all metrics, including EM, BLEU scores, METEOR, and CIDEr, demonstrating its strong effectiveness for 3D question answering.

Table 8: Performance comparison on the validation set of ScanQA [2]. EM indicates exact match accuracy, and B-1, B-2, B-3, B-4 denote BLEU-1, -2, -3, -4, respectively.

Method	EM	B-1	B-2	B-3	B-4	ROUGE-L	METEOR	CIDEr
ScanQA [2]	21.05	30.24	20.40	15.11	10.08	33.33	13.14	64.86
3D-VisTA [51]	22.40	–	–	–	10.40	35.70	13.90	69.60
Oryx-34B [26]	–	38.00	24.60	–	–	37.30	15.00	72.30
LLaVA-Video-7B [46]	–	39.71	26.57	9.33	3.09	44.62	17.72	88.70
3D-LLM (Flamingo) [19]	20.40	30.30	17.80	12.00	7.20	32.30	12.20	59.20
3D-LLM (BLIP2-flant5) [19]	20.50	39.30	25.20	18.40	12.00	35.70	14.50	69.40
Chat-3D [39]	–	29.10	–	–	6.40	28.50	11.90	53.20
NaviLLM [49]	23.00	–	–	–	12.50	38.40	15.40	75.90
LL3DA [7]	–	–	–	–	13.53	37.31	15.88	76.79
Scene-LLM [13]	27.20	43.60	26.80	19.10	12.00	40.00	16.60	80.00
LEO [21]	–	–	–	–	11.50	39.30	16.20	80.00
Grounded 3D-LLM [8]	–	–	–	–	13.40	–	–	72.70
ChatScene [20]	21.62	43.20	29.06	20.57	14.31	41.56	18.00	87.70
LLaVA-3D [50]	27.00	–	–	–	14.50	50.10	20.70	91.70
Video 3D-LLM [48]	30.10	47.05	31.70	22.83	16.17	49.02	19.84	102.06
3DRS (Ours)	30.30	48.37	32.67	23.79	17.22	49.82	20.47	104.78

SQA3D. In Tab. 9, 3DRS achieves the highest scores on the SQA3D test set, outperforming all previous approaches on almost every question type as well as in the overall average, which demonstrates its superior capability for 3D question answering across diverse scenarios.

Scan2cap. In Tab. 10, 3DRS achieves the best performance on the Scan2Cap validation set in terms of CIDEr (C), and remains highly competitive on other metrics such as BLEU-4, METEOR, and ROUGE-L, demonstrating strong overall effectiveness for 3D captioning.

A.4 Qualitative Results

Figs. 5 and 6 provide a visual summary of how our method performs on three challenging 3D scene understanding tasks. These tasks include identifying objects based on language, generating descriptions for specific regions, and answering spatial questions about the scene.

In the visual grounding examples at the top, the model is challenged to find the correct object in a complex 3D environment based on a textual description. The comparison highlights three bounding boxes for each case: blue for the ground truth, red for the baseline, and green for our result. Our

Table 9: Performance comparison on the test set of SQA3D [27].

Method	Test set						Avg.
	What	Is	How	Can	Which	Others	
SQA3D [27]	31.60	63.80	46.00	69.50	43.90	45.30	46.60
3D-VisTA [3]	34.80	63.30	45.40	69.80	47.20	48.10	48.50
LLaVA-Video[46]	42.70	56.30	47.50	55.30	50.10	47.20	48.50
Scene-LLM [13]	40.90	69.10	45.00	70.80	47.20	52.30	54.20
LEO [21]	–	–	–	–	–	–	50.00
ChatScene [20]	45.40	67.00	52.00	69.50	49.90	55.00	54.60
LLaVA-3D [50]	–	–	–	–	–	–	55.60
Video 3D-LLM [48]	51.10	72.40	55.50	69.80	51.30	56.00	58.60
3DRS (Ours)	54.40	75.20	57.00	72.20	49.90	59.00	60.60

Table 10: Performance comparison on the validation set of Scan2Cap [9].

Method	@0.5			
	C	B-4	M	R
Scan2Cap [9]	39.08	23.32	21.97	44.48
3DJCG [3]	49.48	31.03	24.22	50.80
D3Net [5]	62.64	35.68	25.72	53.90
3D-VisTA [51]	66.90	34.00	27.10	54.30
LL3DA [7]	65.19	36.79	25.97	55.06
LEO [21]	68.40	36.90	27.70	57.80
ChatScene [20]	77.19	36.34	28.01	58.12
LLaVA-3D [50]	79.21	41.12	30.21	63.41
Video 3D-LLM [48]	83.77	42.43	28.87	62.34
3DRS (Ours)	86.11	41.63	28.97	62.29

predictions consistently align with the intended targets, showing our model's ability to accurately interpret spatial and semantic cues from language.

The object captioning section in the middle presents how each model describes a highlighted object or area. For each instance, the ground truth, baseline output, and our generated caption are shown, along with their respective CIDEr scores. Our model's captions are both more precise and more faithful to the scene's content, as reflected in the higher evaluation scores.

At the bottom, the question answering task demonstrates the model's reasoning abilities within a 3D environment. The figures show the posed question, the correct answer, the baseline's response, and our model's answer. Even for questions that require counting or locating objects, our approach tends to provide accurate answers, often supported by clear visual evidence in the scene.

Altogether, these qualitative results illustrate that our approach delivers more reliable scene understanding across a variety of tasks, outperforming the baseline in both accuracy and descriptive quality.

A.5 Broader Impacts

Positive impacts. The advancement of 3D perception in AI systems holds significant positive societal potential. Enhanced 3D understanding can benefit applications such as assistive robotics for the elderly and disabled, safer autonomous navigation, improved medical imaging, and immersive educational tools. These technologies have the capacity to improve quality of life, boost accessibility, and enable new forms of human-computer interaction.

Negative impacts. However, the adoption of enhanced 3D perception also raises important privacy concerns, especially in surveillance and monitoring contexts where individuals' activities or environments could be reconstructed and analyzed without their consent. To address these risks, it is crucial to apply robust data anonymization methods—such as blurring faces or removing identifiable features—ensure informed consent from data subjects, enforce strict access controls and data security protocols, and adhere to relevant privacy regulations to protect individual rights.

A.6 Limitation

While our paper aims to enhance the 3D-awareness of MLLMs, the relatively limited size of the dataset used for finetuning—especially when compared to that used during the MLLM pretraining stage—may restrict the full realization of our approach's potential. Consequently, the improvements demonstrated in this work may only represent an initial step toward more robust 3D understanding. A promising direction for future research is to incorporate 3D-awareness learning into the pretraining stage of MLLMs, which could lead to fundamentally stronger models with deeper 3D comprehension.

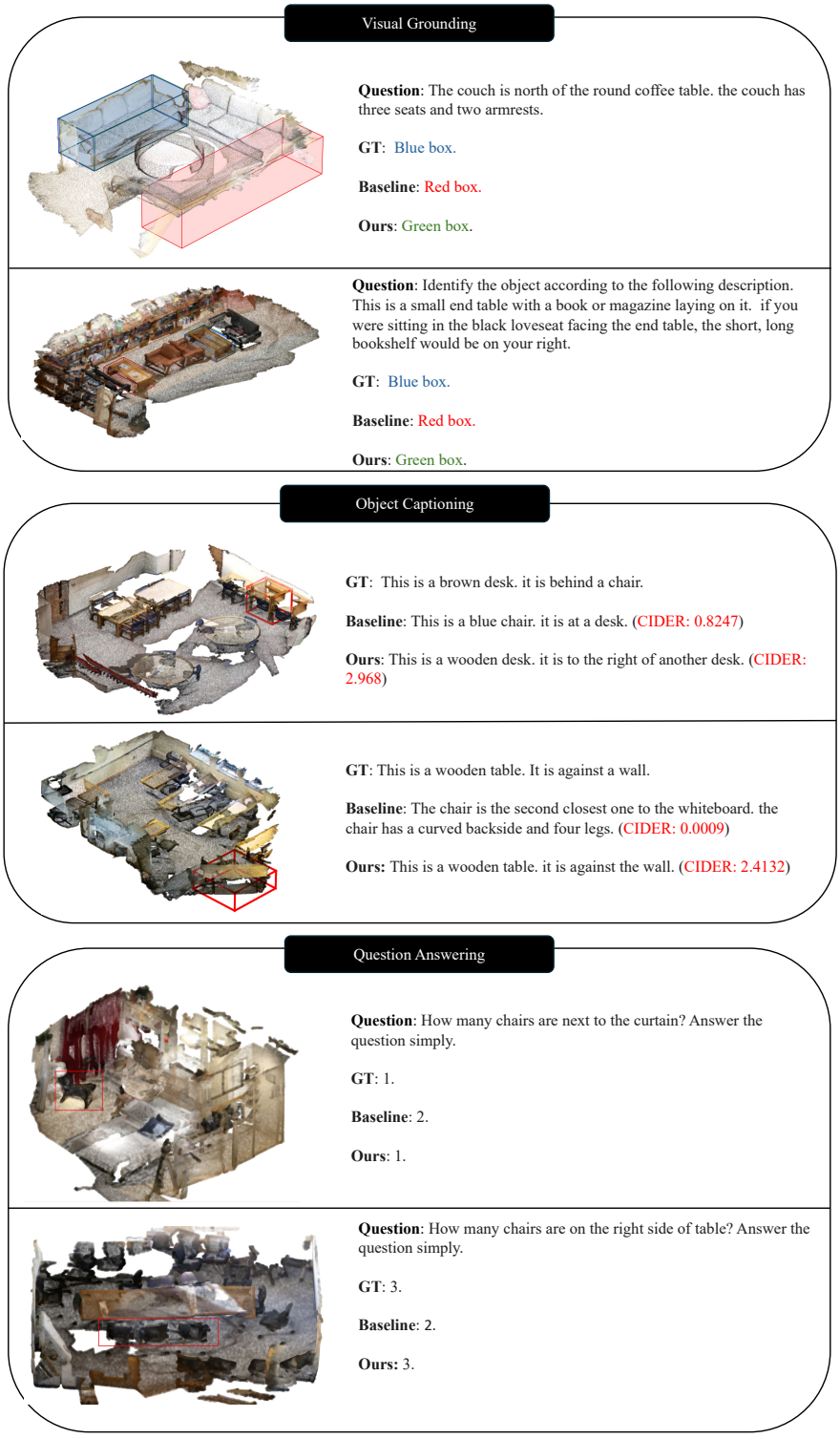

Figure 5: **Visualization of Results Across Different Tasks.** (a) Visual Grounding: The predicted bounding box closely aligns with the ground truth. (b) Object Captioning: Our method generates accurate captions for each referred object. (c) Question Answering: The model provides precise answers, where we use the red rectangles to indicate the visual cues utilized for each response. Best viewed when zoomed in.

Figure 6: **Visualization of Results Across Different Tasks.** (a) Visual Grounding: The predicted bounding box closely aligns with the ground truth. (b) Object Captioning: Our method generates accurate captions for each referred object. (c) Question Answering: The model provides precise answers, where we use the red rectangles to indicate the visual cues utilized for each response. Best viewed when zoomed in.